



# The effect of the electron-donor ability on the OLED efficiency of twisted donor-acceptor type emitters

Dongwook Yang<sup>a,1</sup>, Jae-Min Kim<sup>b,1</sup>, Jin-Suk Huh<sup>b</sup>, Jang-Joo Kim<sup>b,\*\*</sup>, Jong-In Hong<sup>a,\*</sup>

<sup>a</sup> Department of Chemistry, Seoul National University, Seoul, 08826, South Korea

<sup>b</sup> Department of Materials Science and Engineering, Seoul National University, Seoul, 08826, South Korea

## ARTICLE INFO

### Keywords:

Organic light emitting diodes  
Thermally activated delayed fluorescence  
Electron-donor ability

## ABSTRACT

Two twisted donor-acceptor (D-A) chemical structures, CCDMB and PCDMB, were developed as a new class of thermally activated delayed fluorescence (TADF) emitters for organic light-emitting diodes (OLEDs). Two emitters consist of 3-substituted carbazole as a first donor and trivalent boron as an electron acceptor in common, and carbazole and phenoxazine as second donors with different electron donor ability. While PCDMB with a strong phenoxazine donor decreased the lowest singlet excited state ( $S_1$ ) level and thus showed a small singlet-triplet energy difference ( $\Delta E_{ST}$ ) value of 0.13 eV, resulting in effective reverse intersystem crossing (RISC), however, CCDMB with a weak donor showed a large  $\Delta E_{ST}$  value of 0.21 eV. Efficient triplet harvesting of PCDMB was confirmed by a delayed component in transient PL decay curves of 25 wt% PCDMB-doped bis[2-(diphenylphosphino)phenyl] ether oxide (DPEPO) films. OLED devices with a CCDMB emitter showed deep-blue emission with Commission Internationale de l'Éclairage (CIE) of (0.16, 0.12) but a low maximum EQE of 5.5%, indicative of insufficient triplet harvesting. PCDMB-based devices showed green emission with CIE of (0.21, 0.45) and a high maximum EQE of 22.3%. Our study revealed the effect of the electron donor ability of structurally similar emitters on  $\Delta E_{ST}$  values, triplet harvesting, and device efficiency.

## 1. Introduction

Organic light-emitting diodes (OLEDs) have drawn considerable attention since the first report by Tang and Vanslyke [1] and were successfully applied to commercialization in various fields of panel displays including large-screen televisions, smart watches, and smart phones [2]. Fluorescent dopant-based OLEDs can have a maximum internal quantum efficiency (IQE) of up to 25%. On the other hand, phosphorescence emitters which can harvest triplet excitons utilizing spin-orbit coupling of heavy metal atoms raised the maximum IQE up to 100% [3–9]. However, the high cost of commonly used heavy metal atoms such as iridium or platinum increases the price of commercial products and alternative materials are required accordingly.

Metal-free thermally activated delayed fluorescence (TADF) emitters are also capable of using both singlet and triplet excitons, and thus are considered as alternatives to phosphorescence emitters [10,11]. Although typical fluorescence emitters can only utilize excitons in the lowest singlet excited state ( $S_1$ ), TADF emitters can convert 75% of

excitons in the lowest triplet excited state ( $T_1$ ) to the  $S_1$  through reverse intersystem crossing (RISC). Recently, Kim et al. reported deep-blue emitters based on an oxygen-bridged boron acceptor and a spiro-acridine donor with a record external quantum efficiency (EQE) of 28.2% and Commission Internationale de l'Éclairage (CIE)  $y < 0.1$  [12]. Hatakeyama et al. introduced a nitrogen-bridged boron structure with multiple resonance effects, showing deep-blue emission, narrow full-width at half maximum (FWHM) and high EQE [13,14]. Wu et al. reported green TADF materials with a high EQE of 37.8% [15].

Trivalent boron-containing electron acceptors have been utilized in the electron donor (D)-electron acceptor (A) charge-transfer-type TADF emitters due to the vacant p-orbital of the central boron atom that strongly pulls electrons [16]. In addition, the mesityl substituents on boron atom induce distortion of the D-A structure by steric hindrance to decrease the energy gap ( $\Delta E_{ST}$ ) between the  $S_1$  and  $T_1$  by separating the highest occupied molecular orbital (HOMO) and lowest unoccupied molecular orbital (LUMO) of emitters, which can contribute to increase in device efficiency of TADF OLEDs.

\* Corresponding author.

\*\* Corresponding author.

E-mail address: [jihong@snu.ac.kr](mailto:jihong@snu.ac.kr) (J.-I. Hong).

<sup>1</sup> These authors contributed equally to this work.

Herein, we report two TADF emitters, 9-(4-(dimesitylboryl)phenyl)-9H-3,9'-bicarbazole (CCDMB) and 10-(9-(4-(dimesitylboryl)phenyl)-9H-carbazol-3-yl)-10H-phenoxazine (PCDMB), where a triarylborane moiety was used as an electron acceptor, 3-substituted carbazole as a first electron donor in common and carbazole and phenoxazine moieties as second electron donors, respectively (Fig. 1). The double donor system was introduced not only to increase the electron donating ability of two emitters which would induce efficient intramolecular charge transfer (ICT) for radiative decay [17–20] but also to reduce overlap between the HOMO and LUMO by the distortion of two consecutive dihedral angles ( $\alpha_1$  and  $\alpha_2$ , Fig. 1). Our study was focused on interrelations of D-A twist angles, electron-donating ability of D, and OLED device efficiency. CCDMB-based OLED devices showed deep blue CIE coordinates of (0.16, 0.12) but a maximum EQE of 5.5%. On the other hand, PCDMB-based devices exhibited a maximum EQE of 22.3% with green emission (CIE coordinates of (0.21, 0.45)).

## 2. Experimental section

### 2.1. Preparation

#### 2.1.1. Synthesis of 9-benzyl-3-iodo-9H-carbazole (1)

To a stirred solution of 3-iodocarbazole (4.19 g, 14.31 mmol) and tetrabutylammonium iodide (0.53 g, 1.43 mmol) dissolved in 90 ml of dimethyl sulfoxide (DMSO) was added 6 ml of 50% aqueous potassium hydroxide (KOH) solution. To the resulting mixture was injected dropwise benzyl bromide (7.34 g, 42.93 mmol) in 30 ml of DMSO. The resulting mixture was stirred for 2 h, poured into 300 ml of water and extracted with 100 ml of dichloromethane (DCM), dried over anhydrous sodium sulfate ( $\text{Na}_2\text{SO}_4$ ) and concentrated under reduced pressure. The resulting precipitate was recrystallized from 200 ml of methyl alcohol to furnish 9-benzyl-3-iodo-9H-carbazole (5.21 g, 95% yield) as a white solid.  $^1\text{H}$  NMR (300 MHz, chloroform-*d* ( $\text{CDCl}_3$ )):  $\delta$  8.45 (s, 1H), 8.10 (d,  $J = 7.8$  Hz, 1H), 7.70 (d,  $J = 7.8$  Hz, 1H), 7.48 (d,  $J = 7.5$  Hz, 1H), 7.40 (t,  $J = 8.0$  Hz, 2H), 7.35–7.27 (m, 3H), 7.18 (d,  $J = 8.6$  Hz, 1H), 7.14 (d,  $J = 7.4$  Hz, 2H), 5.51 (s, 2H);  $^{13}\text{C}$  NMR (75.47 MHz,  $\text{CDCl}_3$ ):  $\delta$  140.7, 139.8, 136.7, 134.1, 129.3, 128.9, 127.7, 126.6, 126.4, 125.6, 121.8, 120.6, 119.8, 111.1, 109.1, 81.9, 46.6.

#### 2.1.2. Synthesis of 9-benzyl-9H-3,9'-bicarbazole (2)

A mixture of 9-benzyl-3-iodo-9H-carbazole (1, 2.02 g, 6.89 mmol), carbazole (1.73 g, 10.34 mmol), copper sulfate ( $\text{CuSO}_4$ , 0.87 g, 3.45 mmol) and potassium carbonate ( $\text{K}_2\text{CO}_3$ , 3.81 g, 27.6 mmol) dissolved in 15 ml of *o*-dichlorobenzene (*o*-DCB) was refluxed at 180 °C for 12 h. After cooling down to room temperature (RT), the reaction mixture was extracted with DCM (100 ml  $\times$  3). The combined organic layer was dried over anhydrous  $\text{Na}_2\text{SO}_4$  and concentrated under reduced pressure. Purification by silica gel column chromatography ( $\text{SiO}_2$ , *n*-hexane (Hex): DCM = 3:1) gave 9-benzyl-9H-3,9'-bicarbazole (1.74 g, 4.12 mmol, 60% yield).  $^1\text{H}$  NMR (300 MHz,  $\text{CDCl}_3$ ):  $\delta$  8.32 (s, 1H), 8.25 (d,  $J = 7.7$  Hz, 2H), 8.16 (d,  $J = 7.7$  Hz, 1H), 7.59 (t,  $J = 8.5$  Hz, 2H), 7.55 (t,  $J = 12.4$  Hz, 2H), 7.48–7.41 (m, 4H), 7.38–7.33 (m, 6H), 7.30 (d,  $J = 3.0$  Hz, 1H), 7.28 (d,  $J = 2.0$  Hz, 1H), 5.64 (s, 2H);  $^{13}\text{C}$  NMR (75.47 MHz,  $\text{CDCl}_3$ ):  $\delta$  142.1, 141.5, 139.9, 137.0, 129.4, 129.0, 127.8, 126.8, 126.6, 126.0, 125.6, 124.1, 123.3, 122.8, 120.8, 120.5, 119.9, 119.8, 119.7, 110.1, 109.5, 46.9.

#### 2.1.3. Synthesis of 10-(9-benzyl-9H-carbazol-3-yl)-10H-phenoxazine (3)

A mixture of 9-benzyl-3-iodo-9H-carbazole (1, 4.00 g, 10.42 mmol), phenoxazine (2.86 g, 15.63 mmol),  $\text{CuSO}_4$  (1.30 g, 5.22 mmol), and  $\text{K}_2\text{CO}_3$  (4.32 g, 31.26 mmol) in 35 ml of *o*-DCB was refluxed at 180 °C for 12 h. The reaction mixture was cooled down to RT, extracted with DCM (100 ml  $\times$  3), and dried over  $\text{Na}_2\text{SO}_4$ . Purification by silica gel column chromatography ( $\text{SiO}_2$ , Hex:DCM = 3:1) afforded the desired product 3 as a greenish white solid (2.80 g, 6.39 mmol, 61% yield).  $^1\text{H}$  NMR (300 MHz,  $\text{CDCl}_3$ ):  $\delta$  8.19 (d,  $J = 8.3$  Hz, 2H), 7.65 (d,  $J = 8.5$  Hz, 1H), 7.60 (t,

$J = 14.9$  Hz, 1H), 7.52 (d,  $J = 7.9$  Hz, 1H), 7.44–7.37 (m, 5H), 7.33 (d,  $J = 7.5$  Hz, 2H), 6.84 (d,  $J = 7.2$  Hz, 2H), 6.75 (t,  $J = 14.7$  Hz, 2H), 6.68 (d,  $J = 14.7$  Hz, 2H), 6.08 (d,  $J = 7.6$  Hz, 2H), 5.63 (s, 2H)  $^{13}\text{C}$  NMR (75.47 MHz,  $\text{CDCl}_3$ ):  $\delta$  141.2, 140.2, 140.1, 136.8, 133.5, 129.0, 127.7, 126.6, 126.5, 125.0, 123.6, 123.2, 122.6, 121.2, 120.7, 119.8, 113.5, 111.2, 109.3, 46.9, 31.6, 24.1, 22.7.

#### 2.1.4. Synthesis of 9H-3,9'-bicarbazole (4)

To a solution of 9-benzyl-9H-3,9'-bicarbazole (2, 1.74 g, 4.12 mmol) in 80 ml of DMSO was added potassium *tert*-butoxide (*t*-BuOK, 4.62 g, 41.2 mmol) in 20 ml of tetrahydrofuran (THF) at once and subjected to oxygen ( $\text{O}_2$ ) bubbling for 3 h. The resulting mixture was treated with 100 ml of water and stirred for 6 h. The crude mixture was filtered, extracted with DCM (50 ml  $\times$  3), dried over anhydrous  $\text{Na}_2\text{SO}_4$ , and concentrated in vacuo. The desired product 4 was obtained as a white solid (1.26 g, 3.79 mmol, 92% yield).  $^1\text{H}$  NMR (300 MHz,  $\text{CDCl}_3$ ):  $\delta$  8.29 (s, 1H), 8.25 (d,  $J = 1.5$  Hz, 1H), 8.22 (d,  $J = 7.7$  Hz, 2H), 8.09 (d,  $J = 7.8$  Hz, 1H), 7.67 (d,  $J = 8.5$  Hz, 1H), 7.59 (dd,  $J = 1.8, 8.5$  Hz, 1H), 7.53 (d,  $J = 6.4$  Hz, 2H), 7.48–7.39 (m, 4H), 7.34 (d,  $J = 1.7$  Hz, 1H), 7.32 (d,  $J = 11.2$  Hz, 2H);  $^{13}\text{C}$  NMR (75.47 MHz,  $\text{CDCl}_3$ ):  $\delta$  142.0, 140.2, 138.6, 129.4, 126.6, 126.0, 125.5, 124.4, 123.1, 123.0, 120.6, 120.4, 120.0, 119.7, 119.6, 111.7, 111.0, 110.0.

#### 2.1.5. Synthesis of 10-(9H-carbazol-3-yl)-10H-phenoxazine (5)

To a stirred solution of compound 3 (2.80 g, 6.39 mmol) dissolved in 160 ml of DMSO was added *t*-BuOK (7.17 g, 63.90 mmol) in 40 ml of THF and subjected to oxygen bubbling for 3 h. The resulting mixture was filtered, extracted with DCM (50 ml  $\times$  3), dried over anhydrous  $\text{Na}_2\text{SO}_4$ , and concentrated in vacuo to afford compound 5 (2.20 g, 6.31 mmol, 92% yield) as a yellowish white powder.  $^1\text{H}$  NMR (300 MHz,  $\text{CDCl}_3$ ):  $\delta$  8.25 (s, 1H), 8.07 (d,  $J = 8.0$  Hz, 2H), 7.67 (d,  $J = 8.4$  Hz, 1H), 7.51 (d,  $J = 5.9$  Hz, 2H), 7.38 (dd,  $J = 8.4, 1.5$  Hz, 1H), 6.73 (d,  $J = 7.1$  Hz, 2H), 6.65–6.62 (m, 3H), 6.58–6.55 (m, 3H);  $^{13}\text{C}$  NMR (75.47 MHz,  $\text{CDCl}_3$ ):  $\delta$  140.0, 138.9, 131.2, 130.2, 127.1, 126.6, 125.4, 123.4, 123.3, 123.0, 120.6, 120.4, 120.0, 115.4, 113.5, 113.0, 111.0, 110.5.

#### 2.1.6. Synthesis of 9-(4-bromophenyl)-9H-3,9'-bicarbazole (6)

A mixture of 4 (1.26 g, 3.79 mmol), 1-bromo-4-iodobenzene (1.29 g, 4.55 mmol),  $\text{CuSO}_4$  (0.47 g, 1.90 mmol) and  $\text{K}_2\text{CO}_3$  (2.1 g, 15.2 mmol) in 10 ml of *o*-DCB was refluxed for 12 h. The reaction mixture was cooled down to RT and extracted with DCM (50 ml  $\times$  3), dried over anhydrous  $\text{Na}_2\text{SO}_4$ , and concentrated under reduced pressure. The crude product was purified by silica gel column chromatography ( $\text{SiO}_2$ , Hex:DCM = 3:1) to afford 6 (1.20 g, 2.47 mmol, 65% yield).  $^1\text{H}$  NMR (300 MHz,  $\text{CDCl}_3$ ):  $\delta$  8.33 (s, 1H), 8.25 (d,  $J = 7.7$  Hz, 2H), 8.16 (d,  $J = 7.7$  Hz, 1H), 7.84 (d,  $J = 8.5$  Hz, 2H), 7.60–7.56 (m, 4H), 7.52 (d,  $J = 10.1$  Hz, 2H), 7.46–7.42 (m, 4H), 7.39–7.32 (m, 3H);  $^{13}\text{C}$  NMR (75.47 MHz,  $\text{CDCl}_3$ ):  $\delta$  141.9, 141.4, 139.8, 136.5, 133.4, 133.2, 130.2, 128.8, 126.9, 125.9, 125.7, 124.6, 123.2, 123.1, 121.4, 120.7, 120.4, 119.7, 119.6, 110.7, 110.0, 109.8.

#### 2.1.7. Synthesis of 10-(9-(4-bromophenyl)-9H-carbazol-3-yl)-10H-phenoxazine (7)

A mixture of 5 (2.20 g, 6.31 mmol), 1-bromo-4-iodobenzene (2.14 g, 7.57 mmol),  $\text{CuSO}_4$  (0.80 g, 3.20 mmol) and  $\text{K}_2\text{CO}_3$  (3.48 g, 25.2 mmol) dissolved in 20 ml of *o*-DCB was refluxed for 12 h. The reaction mixture was cooled down to RT and extracted into DCM (50 ml  $\times$  3). The combined organic layer was dried over anhydrous  $\text{Na}_2\text{SO}_4$  and concentrated under reduced pressure to afford 7 (2.16 g, 4.29 mmol, 68% yield) after purification by silica gel column chromatography ( $\text{SiO}_2$ , Hex:DCM = 3:1).  $^1\text{H}$  NMR (300 MHz,  $\text{CDCl}_3$ ):  $\delta$  8.16 (d,  $J = 10.0$  Hz, 2H), 7.84 (d,  $J = 8.4$  Hz, 2H), 7.63 (d,  $J = 8.6$  Hz, 1H), 7.57 (d,  $J = 8.4$  Hz, 2H), 7.52–7.45 (m, 2H), 7.71–7.35 (m, 2H), 6.78 (d,  $J = 7.1$  Hz, 2H), 6.69–6.64 (m, 2H), 6.62 (t,  $J = 7.1$  Hz, 2H), 6.04 (d,  $J = 7.4$  Hz, 2H);  $^{13}\text{C}$  NMR (75.47 MHz,  $\text{CDCl}_3$ ):  $\delta$  144.0, 141.2, 140.0, 136.5, 135.2, 133.4, 131.3, 128.8, 128.4, 126.9, 125.6, 123.3, 123.0, 122.9, 121.5, 121.2,

120.8, 120.7, 115.4, 113.5, 112.1, 110.0.

### 2.1.8. Synthesis of 9-(4-(dimesitylboryl)phenyl)-9H-3,9'-bicarbazole (CCDMB) (8)

*n*-Butyllithium solution (1.6 M in Hex, 3.1 ml, 4.94 mmol) was added dropwise via syringe to a solution of **6** (1.20 g, 2.47 mmol) in 12 ml of dry THF at  $-78\text{ }^{\circ}\text{C}$  under nitrogen atmosphere. The resulting mixture was stirred at  $-78\text{ }^{\circ}\text{C}$  for 1 h and treated with fluorodimesitylborane (1.99 g, 7.41 mmol). After 1 h reaction at  $-78\text{ }^{\circ}\text{C}$ , the mixture was slowly warmed up to RT and stirred overnight. The mixture was poured into water, extracted with DCM (50 ml  $\times$  3), dried with anhydrous  $\text{Na}_2\text{SO}_4$  and concentrated *in vacuo*. The crude product was purified by column chromatography ( $\text{SiO}_2$ , Hex:ethylacetate = 20:1) to afford CCDMB (1.20 g, 1.83 mmol, 74%).  $^1\text{H}$  NMR (300 MHz,  $\text{CDCl}_3$ ):  $\delta$  8.31 (d,  $J = 1.6$  Hz, 1H), 8.23 (d,  $J = 7.7$  Hz, 2H), 8.15 (d,  $J = 7.7$  Hz, 1H), 7.85 (d,  $J = 8.1$  Hz, 2H), 7.73–7.67 (m, 3H), 7.60 (d,  $J = 8.4$  Hz, 2H), 7.54 (d,  $J = 7.3$  Hz, 1H), 7.49–7.43 (m, 4H), 7.38–7.30 (m, 3H), 6.91 (s, 4H), 2.37 (s, 6H), 2.15 (s, 12H);  $^{13}\text{C}$  NMR (75.47 MHz,  $\text{CDCl}_3$ ):  $\delta$  141.9, 141.1, 140.9, 140.5, 139.6, 139.0, 138.1, 130.2, 130.1, 128.4, 127.2, 126.8, 126.0, 125.9, 125.6, 124.7, 124.3, 123.2, 120.7, 120.6, 120.3, 119.7, 119.5, 111.1, 110.4, 109.8, 23.6, 21.3; HRMS ( $\text{FAB}^+$ ), calculated for  $\text{C}_{48}\text{H}_{41}\text{BN}_2$  656.3363, found 656.3371.

### 2.1.9. Synthesis of 10-(9-(4-(dimesitylboryl)phenyl)-9H-carbazol-3-yl)-10H-phenoxazine (PCDMB) (9)

To a solution of 10-(9-(4-bromophenyl)-9H-carbazol-3-yl)-10H-phenoxazine (**7**, 2.16 g (4.29 mmol)) in 20 ml of dry THF at  $-78\text{ }^{\circ}\text{C}$  under nitrogen atmosphere was added dropwise 1.6 M *n*-butyllithium solution in Hex (3.22 ml, 5.15 mmol). The resulting mixture was stirred at  $-78\text{ }^{\circ}\text{C}$  for 1 h and treated with fluorodimesityl borane (1.63 g, 6.08 mmol). After 1 h reaction at  $-78\text{ }^{\circ}\text{C}$ , the mixture was gradually allowed to warm up to RT and stirred overnight. The mixture was poured into water, extracted with DCM (50 ml  $\times$  3), dried with anhydrous  $\text{Na}_2\text{SO}_4$  and concentrated under reduced pressure to give a crude product, which was purified by column chromatography ( $\text{SiO}_2$ , Hex:ethyl acetate = 20:1) to afford PCDMB (2.00 g, 2.97 mmol, 69% yield) as a yellowish white powder.  $^1\text{H}$  NMR (300 MHz,  $\text{CDCl}_3$ ):  $\delta$  8.13 (d,  $J = 8.3$  Hz, 2H), 7.82 (d,  $J = 8.1$  Hz, 2H), 7.70 (d,  $J = 8.3$  Hz, 1H), 7.65 (d,  $J = 8.2$  Hz, 2H), 7.56–7.46 (m, 2H), 7.37 (d,  $J = 7.8$  Hz, 2H), 6.90 (s, 4H), 6.74 (d,  $J = 7.2$  Hz, 2H), 6.66–6.58 (m, 4H), 6.00–5.98 (m, 2H), 2.53 (s, 6H), 2.13 (s, 12H);  $^{13}\text{C}$  NMR (75.47 MHz,  $\text{CDCl}_3$ ):  $\delta$  145.2, 141.6, 141.0, 140.9, 140.5, 139.8, 139.3, 139.1, 139.0, 138.1, 138.0, 134.7, 128.8, 128.4, 126.9, 126.8, 126.0, 125.9, 125.8, 123.2, 120.8, 120.7, 113.6, 112.4, 110.4, 112.3, 23.6, 21.3; HRMS ( $\text{FAB}^+$ ), calculated for  $\text{C}_{48}\text{H}_{41}\text{BN}_2\text{O}$  672.3312, found 672.3320.

### 2.1.10. Device fabrication

In the course of device fabrication, a pre-patterned 70 nm thick indium-doped tin oxide (ITO) was cleaned with deionized water, acetone, and isopropyl alcohol. All layers were vacuum-deposited and encapsulated in  $\text{N}_2$  glove box without being exposed to external air.

## 2.2. Measurements

### 2.2.1. Calculations

Density functional theory (DFT) calculations were performed using the ORCA program package to estimate charge distribution, frontier molecular orbital energy levels and dihedral angles. Gas-phase geometry optimizations for the  $\text{S}_1$  and  $\text{T}_1$  were carried out with time-dependent density functional theory (TD-DFT) calculations at the B3LYP functional and 6-31G\* basis set. Natural transition orbitals (NTOs) analysis was performed using the Jaguar quantum chemical calculation code in the Schrodinger Materials Science Suite. The functional used in the calculation was  $\omega\text{B97X-D}$  ( $\omega = 0.1$ ).

### 2.2.2. Photophysical measurements

The Ultraviolet (UV) spectra were recorded on a Beckman DU650 spectrophotometer. Fluorescence spectra were recorded on a Jasco FP-6500 spectrophotometer and Photon Technology International, Inc. spectrofluorometer. Thin films were excited by a xenon lamp (300 and 350 nm) operating with an Acton Research Co. monochromator. Transient PL measurements were carried out by excitation using  $\text{N}_2$  laser from Usho Optical Systems Co. (337 nm). Photoluminescence (PL) decay was recorded by Hamamatsu C10627 streak camera as a detector. In analysis of angle-dependent PL spectrum, thin film on the fused silica substrate was attached to half-cylinder lens using index matching liquid. P-polarized spectra were measured depending on angle by combination of rotational stage and Maya 200 Pro (Ocean Optics Inc.) detector at RT. Low-temperature measurements were conducted using a cryostat (Iwatani Industrial Gases, CRT-006-2000) with application of an InGa alloy as an adhesive to ensure good thermal conductivity between the silicon substrate and the sample holder.

### 2.2.3. Electrochemical measurements

Cyclic voltammetry (CV) experiments were conducted in DCM solution (1.00 mM) with 0.1 M tetra-*n*-butylammonium hexafluorophosphate ( $\text{TBAPF}_6$ ) as the supporting electrolyte (VSP Princeton Applied Research). A platinum disk electrode was employed as the working electrode and referenced to a ( $\text{Ag}/\text{Ag}^+$ ) reference electrode. The HOMO levels were calibrated by using the HOMO level of  $\text{N,N}'$ -Di(1-naphthyl)- $\text{N,N}'$ -diphenyl-(1,1'-biphenyl)-4,4'-diamine (NPB) as a reference material.

### 2.2.4. Characterization

Both  $^1\text{H}$  and  $^{13}\text{C}$  NMR spectra were recorded in  $\text{CDCl}_3$  on a Bruker AM 300 spectrometer.  $^1\text{H}$  NMR chemical shifts in  $\text{CDCl}_3$  were referenced to  $\text{CHCl}_3$  (7.283 ppm) and  $^{13}\text{C}$  NMR chemical shifts in  $\text{CDCl}_3$  were also reported relative to  $\text{CHCl}_3$  (77.23 ppm). High-resolution mass analyses (JEOL, JMS-700) with fast atom bombardment (FAB) positive mode and electron impact (EI) were recorded from the National Centre for Inter-University Research Facilities.

### 2.2.5. Thermal stability

The thermal decomposition temperature ( $T_g$ ) values of CCDMB and PCDMB were measured using differential scanning calorimetry (DSC, DSC Q10, TA Instruments). The  $T_g$  value of CCDMB was  $112\text{ }^{\circ}\text{C}$  and that of PCDMB was  $131\text{ }^{\circ}\text{C}$ , indicating their thermal stability.

### 2.2.6. Device performance measurements

Current density-voltage-luminance was measured by using Photo Research PR650 spectrometer and Keithley 2400 source meter.

## 3. Results and discussion

### 3.1. Computational results

Both DFT and TD-DFT calculations were carried out using the B3LYP functional and 6-31G\* basis set, utilizing corresponding effective core potentials as employed in the ORCA package. Molecular structures, charge distributions of the HOMO/LUMO levels and HOMO-LUMO energy gap ( $E_g$ ) of CCDMB and PCDMB are depicted on Fig. 1. The distorted structure between D and A promoted charge separation of HOMO-LUMO energy levels, resulting in small energy differences between  $\text{S}_1$  and  $\text{T}_1$  ( $\Delta E_{\text{ST}}$ ). Calculation results are summarized in Table 1.  $\Delta E_{\text{ST}}$  values of CCDMB and PCDMB are 0.122 eV and 0.001 eV, respectively and are adequate for RISC (generally under 0.2 eV for efficient triplet harvesting) which is a key factor for TADF mechanism. However, two molecules showed different dihedral angles ( $\alpha_1$ ) between the 3-substituted carbazole (first donor) and the carbazole or phenoxazine (second donor). While  $\alpha_1$  of CCDMB is  $59.1^{\circ}$ , the plane of phenoxazine in PCDMB is almost orthogonal to that of the 3-substituted carbazole with a

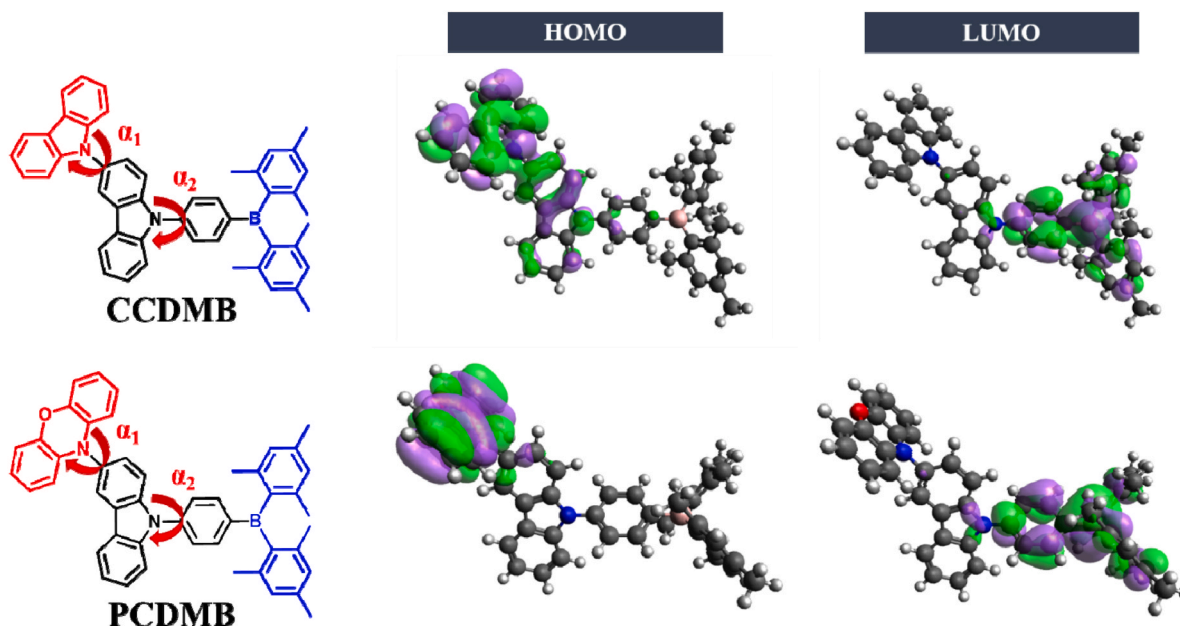


Fig. 1. Molecular structures and charge distributions of CCDMB and PCDMB.

**Table 1**  
Calculated energy levels and twist angles of CCDMB and PCDMB.

Emitter	HOMO [eV]	LUMO [eV]	$E_g$ [eV]	$S_1$ [eV]	$T_1$ [eV]	$\Delta E_{ST}$ [eV]	$\alpha_1$ [°]	$\alpha_2$ [°]
CCDMB	-5.04	-1.81	3.23	2.901	2.779	0.122	59.1	52.9
PCDMB	-4.42	-1.82	2.60	2.320	2.319	0.001	87.0	53.7

dihedral angle of 87.0°, which would lead to charge separation and thus decrease  $\Delta E_{ST}$ . In accordance with our expectations, PCDMB showed a smaller charge overlap between the HOMO and LUMO than CCDMB, resulting in smaller  $\Delta E_{ST}$ . This can be explained by charge density distributions on the HOMO levels of both compounds as depicted in Fig. 1. Charges on the HOMO level of CCDMB were mainly localized on the edge-carbazole, reaching the 3-substituted carbazole (first donor). On the other hand, PCDMB showed the charge population almost on the edge-phenoxazine, not on the 3-substituted carbazole, indicating that the phenoxazine unit acted as a main donor in PCDMB. Therefore, CCDMB allowed charge density overlap between the HOMO and LUMO to cause efficient interactions between D and A, resulting in larger  $\Delta E_{ST}$ .

### 3.2. Synthesis

The synthetic route is illustrated in Scheme 1. Synthesis of CCDMB and PCDMB started with N-benzyl protection of 3-iodocarbazole. The second electron donor moieties, carbazole and phenoxazine, were linked to N-benzylated 3-iodocarbazole by the Ullmann coupling reaction to yield **2** and **3**, respectively. After removal of a benzyl moiety, para-disubstituted benzene was directly connected to the carbazole of **4** and **5** by the Ullmann coupling reaction to afford **6** and **7**. Finally, dimesitylboron fluoride was linked to **6** and **7** through anionic coupling reaction using *n*-butyllithium to furnish CCDMB and PCDMB, respectively, which were characterized by  $^1\text{H}$  NMR,  $^{13}\text{C}$  NMR and high-resolution mass analyses.

### 3.3. Photophysical properties

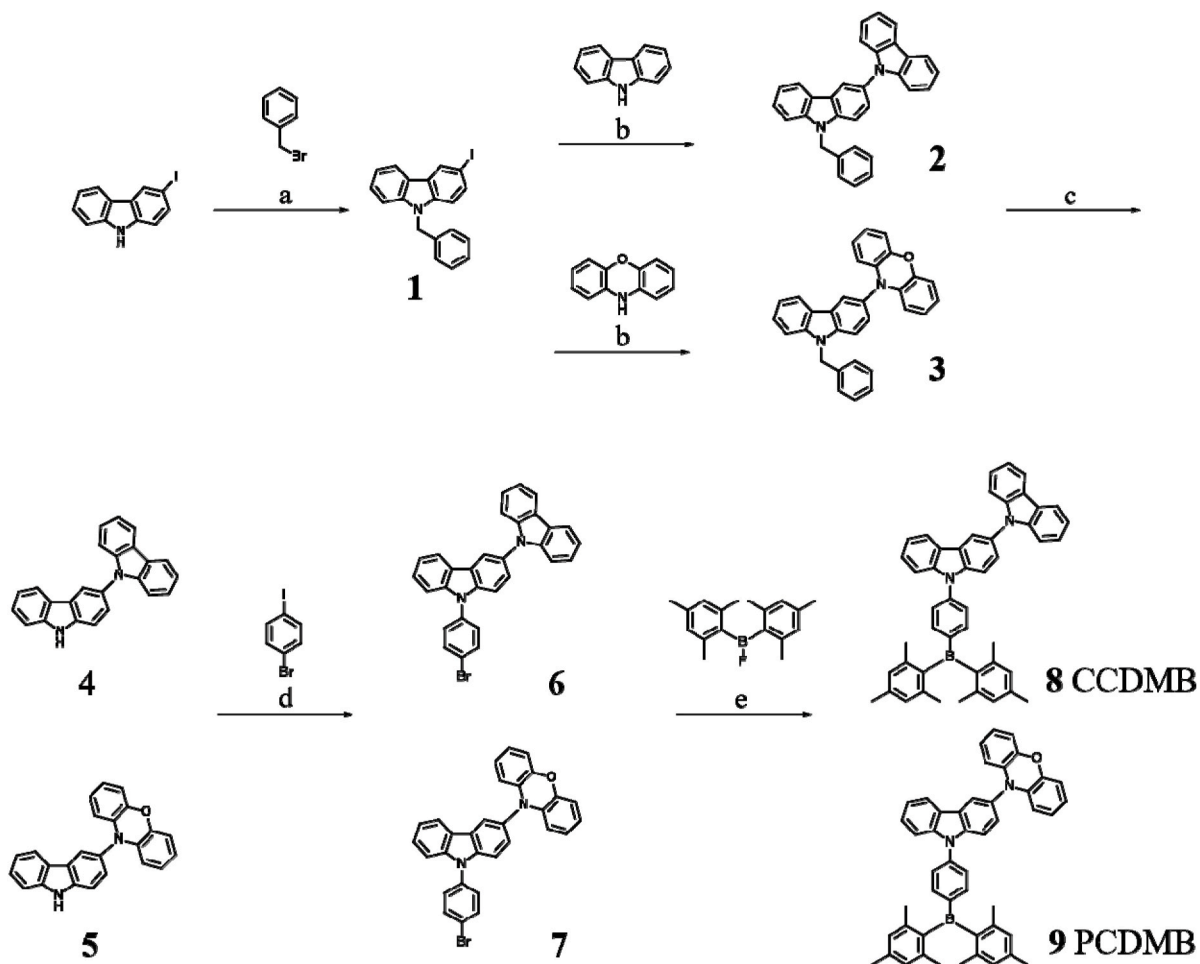
#### 3.3.1. Photophysical properties in solution

The UV and PL spectra of CCDMB and PCDMB in solution are depicted in Fig. 2 and summarized in Table 2. The UV spectra were

obtained in toluene (Tol) (0.02 mM). CCDMB showed two types of absorption bands; sharp band under 310 nm ( $\pi$ - $\pi^*$  transition) and broad band in range of 310–400 nm (ICT transition) (Fig. 2(a)). For PCDMB emitter, the peaks from the  $\pi$ - $\pi^*$  transition emerged under 300 nm and band from the ICT transition appeared in 300–400 nm region (Fig. 2(b)). Fig. 2(a) and (b) showed the PL spectra of CCDMB and PCDMB, respectively, under various solvent conditions (Hex, Tol, chloroform (CF), THF, DCM, methanol (MeOH), and acetonitrile (ACN)). CCDMB and PCDMB showed bathochromic shifts with increasing solvent polarity. The charge transfer singlet state ( $^1\text{CT}$ ) energy level decreases as the solvent polarity increases due to strong interaction between the solvent field and  $^1\text{CT}$  state, and is accompanied by large Stokes shift along with decreased PL intensity (Fig. S1) [21].

As shown in Fig. S1 the PL intensity of CCDMB decreased by 20% in Tol, 44% in CF, 60% in both THF and DCM, 82% in MeOH and 85% in ACN, compared to that in Hex. On the other hand, the PL intensity of PCDMB showed much more outstanding quenching degree of 46% in Tol, 84% in CF and almost completely quenched in THF (98%) and DCM (96%), compared to that in Hex. PCDMB showed complete emission quenching in highly polar MeOH and ACN solvent, which is normally observed in molecules with strong ICT character. [22–24] Please note that the stronger CT character of PCDMB should result from the stronger electron-donor ability of phenoxazine [25]. The shoulder peaks which emerge in polar solvents (CF, THF, DCM, MeOH, and ACN; Fig. 2(a) and (b)) are derived from the  $^1\text{LE}$  state which is unaffected by the solvent polarity. While the  $^1\text{CT}$  emission intensity decreases with the increasing solvent polarity, the  $^1\text{LE}$  emission intensity remains low irrespective of the solvent polarity, which results in a dual emission [23].

The relationship between solvent-dependent Stokes shift ( $\nu_a - \nu_f$ ) and transition dipole moment can be explained by the Lippert-Mataga equation [26].



**Scheme 1.** Synthetic routes to CCDMB and PCDMB. (a) 50% KOH, tetrabutylammonium iodide; (b) CuSO<sub>4</sub>, K<sub>2</sub>CO<sub>3</sub>, *o*-DCB; (c) *t*-BuOK, O<sub>2</sub> bubbling, DMSO/THF/H<sub>2</sub>O; (d) CuSO<sub>4</sub>, K<sub>2</sub>CO<sub>3</sub>, *o*-DCB; (e) *n*-BuLi, THF.

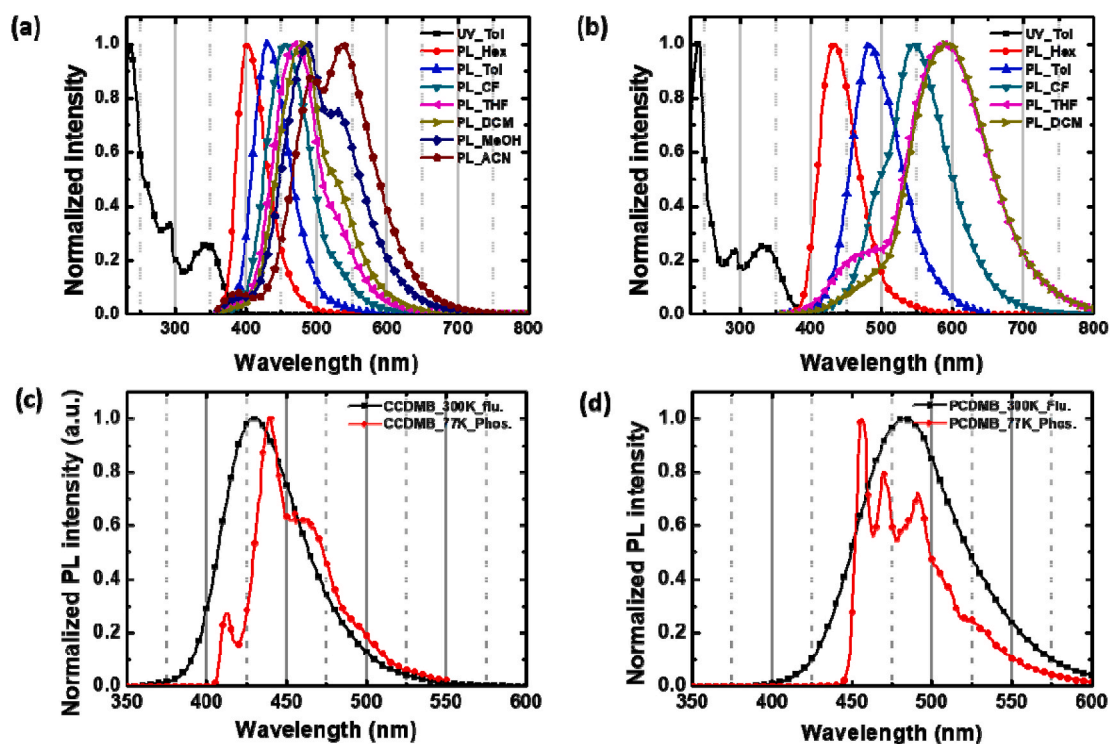


**Fig. 2.** Normalized absorption and emission spectra of (a) CCDMB (0.02 mM) and (b) PCDMB (0.02 mM) in various solvents; fluorescence and phosphorescence spectra of (c) CCDMB and (d) PCDMB in Tol (0.02 mM).

**Table 2**  
Summary of photophysical properties of CCDMB and PCDMB in various solvents.

Solvents	Tol <sup>a</sup> (nm)	Hex <sup>b</sup> (nm)	Tol <sup>b</sup> (nm)	CF <sup>b</sup> (nm)	THF <sup>b</sup> (nm)	DCM <sup>b</sup> (nm)	MeOH <sup>b</sup> (nm)	ACN <sup>b</sup> (nm)	S <sub>1</sub> <sup>c</sup> (eV)	T <sub>1</sub> <sup>d</sup> (eV)	ΔE <sub>ST</sub> (eV)
CCDMB	343	402	431	456	469	479	487	537	3.26	3.05	0.21
PCDMB	331	433	484	546	589	590	–	–	2.90	2.77	0.13

<sup>a</sup> Maximum UV wavelength ( $\lambda_{\max, UV}$ ).

<sup>b</sup> Maximum PL wavelength ( $\lambda_{\max, PL}$ ).

<sup>c</sup> Determined with onset of PL spectrum in Tol at 300 K.

<sup>d</sup> Determined with onset of PL spectrum in Tol at 77 K with 20 ms time delay.

$$hc(\nu_a - \nu_f) = hc(\nu_a^0 - \nu_f^0) + \frac{2(\mu_e - \mu_g)^2}{a^3} f(\epsilon, n)$$

where  $f(\epsilon, n)$  is the orientation polarizability of the solvent,  $\nu_a^0 - \nu_f^0$  is the Stokes shift when  $f$  is zero,  $a$  represents the solvent Onsager cavity radius,  $\epsilon$  and  $n$  are solvent dielectric index and the solvent refractive index, respectively. The dipole moments of each molecule were 3.7 D ( $\mu_g$ ) and 18.6 D ( $\mu_e$ ) for CCDMB, 0.9 D ( $\mu_g$ ) and 22.1 D ( $\mu_e$ ) for PCDMB. The  $\mu_e$  value of PCDMB is very close to that of 4-(*N,N*-dimethylamino)-benzonitrile (DMABN), a well-known effective CT molecule with  $\mu_e$  of 23 D [27]. The  $\mu_e - \mu_g$  of PCDMB was 21.2 D, much bigger than that of CCDMB (14.9 D). This indicates the fact that the larger the solvent polarity is, the larger bathochromic shift PCDMB shows. It has been known

**Table 3**  
Summary of photophysical properties of 25 wt% CCDMB- and PCDMB-doped DPEPO films.

DPEPO: 25 wt% Emitter	$\lambda_{\max, UV}$ (nm)	$\lambda_{\max, PL}$ (nm) <sup>a</sup>	Dipole orientation (%)	PLQY (%)
CCDMB	343	436	76	63
PCDMB	333	493	70	65

<sup>a</sup> Excitation wavelength: 325 nm.

that the large  $\mu_e - \mu_g$  enhances the RISC rate, leading to higher TADF efficiency (*vide supra*) [28–30].

To estimate experimental values of  $\Delta E_{ST}$  and predict the possibility of triplet exciton harvesting by up-conversion, fluorescence spectra (300 K; Flu.) and phosphorescence spectra (77 K, 20 ms time delay; Phos.) were recorded in Tol and depicted in Fig. 2(c) and (d). To understand phosphorescence behaviour of CCDMB and PCDMB, individual phosphorescence of each donor unit was also measured and collected in Fig. S2. Phosphorescence spectra of both CCDMB and PCDMB in frozen Tol indicate the locally excited triplet (<sup>3</sup>LE) state and well accord with those of donors because the lowest triplet levels of donors are lower than that of acceptor [31]. The  $\Delta E_{ST}$  value of CCDMB (0.21 eV) is larger than that of PCDMB (0.13 eV) which agrees with the calculation data (Table 1) as listed in Table 2. This resulted from the stronger donating ability of phenoxazine than carbazole and thus lowered S<sub>1</sub> level of PCDMB, leading to decreased  $\Delta E_{ST}$ . It was previously known that the donor with strong donating ability has lower S<sub>1</sub> level [17,32]. Consequently, S<sub>1</sub> state of PCDMB was 2.90 eV, much lower than that of CCDMB (3.26 eV), leading to much smaller  $\Delta E_{ST}$  value of PCDMB.

### 3.3.2. Photophysical properties of doped films

The film state absorbance and PL spectra of 25 wt% CCDMB and PCDMB doped in bis[2-(diphenylphosphino)phenyl] ether oxide (DPEPO) host are shown in Fig. 3(a). The  $\lambda_{\max, UV}$  of CCDMB and PCDMB

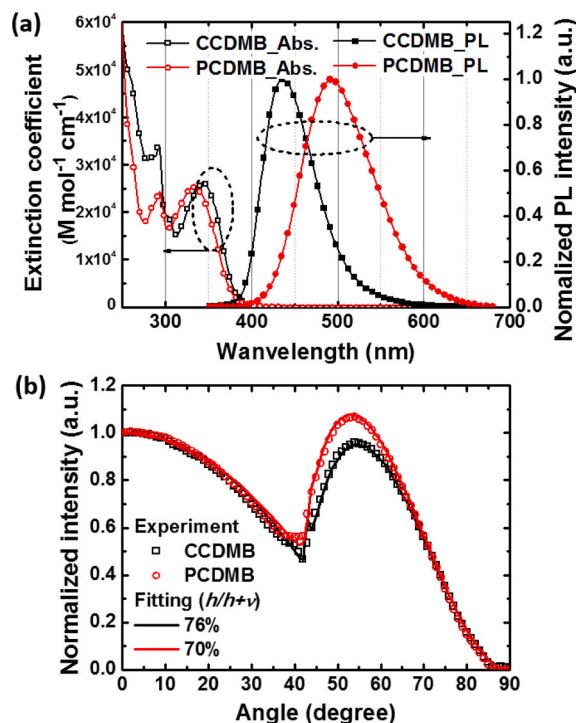


**Fig. 3.** (a) Absorbance and PL spectra, (b) angle-dependent PL intensity of p-polarized light of films of 25 wt% CCDMB and PCDMB doped in DPEPO.

were recorded at 343 and 333 nm, and  $\lambda_{\max, PL}$  values were 434 and 493 nm, respectively. It is known that the out-coupling efficiency of OLED emitters are closely related to their dipole orientation; in particular, emitters with high degrees of horizontal orientation of transition dipole moments have great potential to achieve highly efficient OLEDs [33]. Angle-dependent PL intensities were analyzed to determine dipole orientation of the emitters. The p-polarized PL intensity depending on the emission angle was measured at the  $\lambda_{\max, PL}$  of each emitter and is depicted in Fig. 3(b). Horizontal transition dipole ratio, which is the ratio of the horizontal direction to all 3-dimensional directions, was

values of the device since PLQYs are measured under photoexcited state, which does not consider triplet harvesting.

Delayed fluorescence was measured with transient PL spectroscopy. The delayed component with  $\sim\mu\text{s}$  scale lifetime exists both in CCDMB and PCDMB, however that of CCDMB showed very low intensity and completely quenched after 1  $\mu\text{s}$ , which indicates its inefficient RISC and is consequently unfavourable for triplet harvesting. On the other hand, the delayed component of PCDMB is large enough for sufficient triplet harvesting to run TADF mechanism. The prompt fluorescence lifetimes are 7.4 and 26.2 ns for CCDMB and PCDMB, respectively and delayed

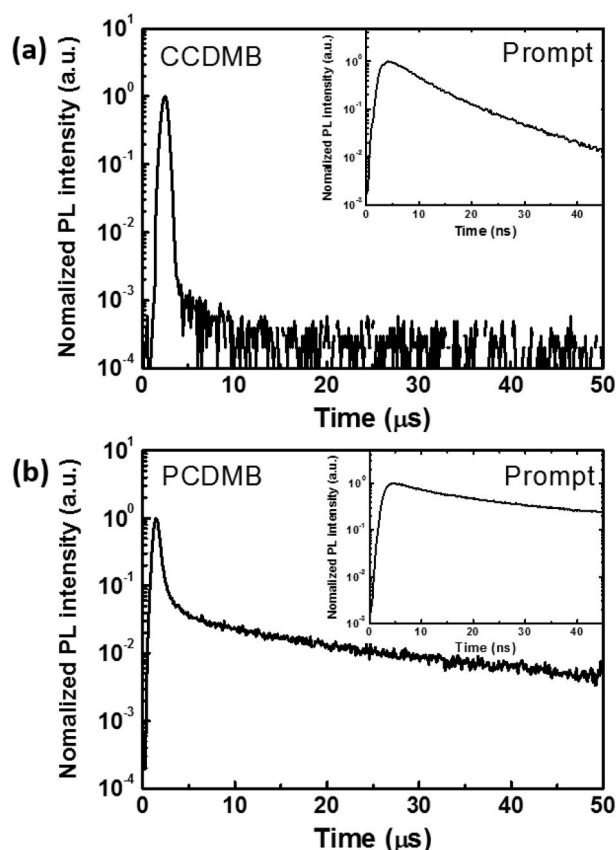


Fig. 4. Transient PL decay curve of 25 wt% (a) CCDMB and (b) PCDMB doped in DPEPO.

calculated to be 76% for CCDMB and 70% for PCDMB, indicating that horizontally oriented emitters become dominant [34]. PL quantum yields (PLQYs) were measured using an integrating sphere and a continuous wave He/Cd laser (325 nm). The PLQYs of CCDMB- and PCDMB-doped DPEPO films were 63% and 65%, respectively, for the doping ratio of 25 wt%. The PLQY values are summarized in Table 3. Note that the PLQY values are not directly connected with the EQE

fluorescence lifetime for PCDMB is 23.2  $\mu\text{s}$ . The decay curve of CCDMB is better fitted to single component exponential decay, since the intensity of the delayed fluorescence is low. To confirm the TADF properties of CCDMB and PCDMB, the temperature-dependent transient PL experiments were performed from 100 K to 300 K, as shown in Fig. S3. The prompt decay curves of two molecules were almost overlapped irrespective of the temperature change. The delayed decay curves of CCDMB

Table 4

Device performance of OLEDs.

EML (DPEPO host)	EQE (%)		Current efficiency (cd/A)		Power efficiency (lm/W)		Turn-on Voltage (V)	CIE (x, y) <sup>a</sup>
	Max	400 cd/m <sup>2</sup>	Max	400 cd/m <sup>2</sup>	Max	400 cd/m <sup>2</sup>		
CCDMB 15 wt%	2.1	–	1.7	–	1.0	–	5.4	0.17, 0.14
CCDMB 25 wt%	5.5	–	3.8	–	3.1	–	3.9	0.16, 0.12
PCDMB 15 wt%	19.8	1.5	44.2	3.4	35.7	1.1	3.9	0.19, 0.38
PCDMB 25 wt%	22.3	6.6	57.8	17.0	50.5	8.5	3.6	0.21, 0.45

<sup>a</sup> at the current density of 1 mA/cm<sup>2</sup>.

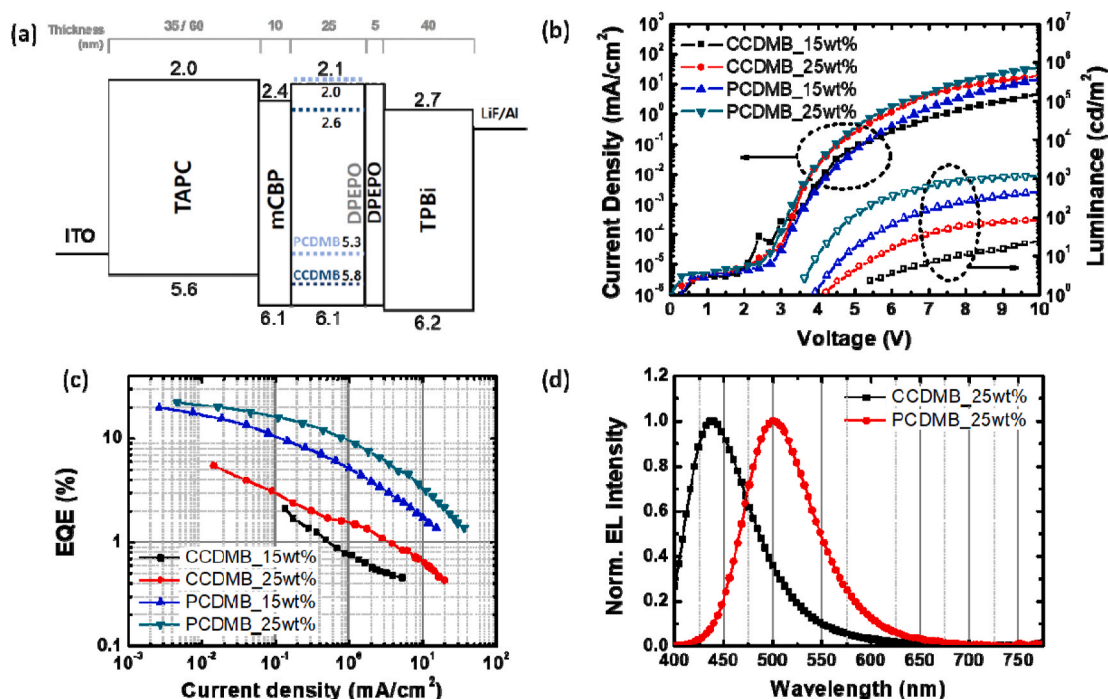


Fig. 5. (a) Device structure of OLEDs, (b) current density-voltage-luminance ( $J$ - $V$ - $L$ ) characteristics, (c) EQE vs. luminance (EQE- $L$ ), and (d) normalized electroluminescence (EL) intensities at the current density of  $1 \text{ mA/cm}^2$ .

remained unchanged, indicating lack of triplet harvesting. However, the delayed component of PCDMB showed evident increase with the increasing temperature, indicating its harvesting of triplet excitons. The large difference in transient PL of structurally similar CCDMB and PCDMB was due to the stronger electron donating ability of phenoxazine than carbazole by virtue of electron lone-pairs on the oxygen atom of phenoxazine. The strong electron donating ability of phenoxazine not only reduced the  $S_1$  level of PCDMB that led to small  $\Delta E_{ST}$  value of 0.13 but also caused large  $\mu_e - \mu_g$  of 21.2 D which additionally facilitated triplet harvesting by effective RISC as mentioned above [28–30]. Equations for rate constants are demonstrated in Equation S1 and details are demonstrated in Table S1.

### 3.4. Electrochemical and thermal properties

The energy levels of CCDMB and PCDMB were confirmed by CV analysis. The HOMO/LUMO levels of CCDMB and PCDMB were estimated to be 5.25/1.95 and 4.75/1.50, respectively. The thermal decomposition temperature ( $T_g$ ) values of CCDMB and PCDMB were measured with differential scanning calorimetry (DSC). The  $T_g$  value of CCDMB was  $112 \text{ }^\circ\text{C}$  and that of PCDMB was  $131 \text{ }^\circ\text{C}$ , indicating their thermal stability. CV voltammograms and DSC thermograms are depicted in Fig. S4. The HOMO/LUMO and  $T_g$  values are listed in Table S2.

### 3.5. Device performance

OLED devices were fabricated using DPEPO as a single host with varying dopant concentrations of 15–25 wt% (Fig. 5). 4,4'-Cyclohexylidenebis[ $N,N$ -bis(4-methylphenyl)benzenamine] (TAPC) was used as a hole transporting material, 3,3-di(9H-carbazol-9-yl)biphenyl (mCBP) and DPEPO intrinsic layers were embedded as triplet blocking layers. For efficient electron transport to the shallow-lying LUMO of DPEPO, 2,2',2''-(1,3,5-benzinetriyl)-tris(1-phenyl-1- $H$ -benzimidazole) (TPBi) was introduced. Lithium fluoride (LiF) and aluminum (Al) were introduced as the electron injecting layer and the metal electrode, respectively. The device structure is ITO (70 nm)/TAPC (35, 60 nm)/

mCBP (10 nm)/DPEPO:dopant (15, 25 wt%, 25 nm)/DPEPO (5 nm)/TPBi (40 nm)/LiF (1 nm)/Al (100 nm) (Fig. 5(a)). The thickness of TAPC should be different (35 nm for CCDMB; 60 nm for PCDMB, respectively) in two devices considering different PL spectra of two dopants to maximize the outcoupling efficiency. Device performances are listed in Table 4. Both devices showed increasing current density and luminance in the voltage range after the built-in potential with increasing doping concentration (Fig. 5(b)). On the other hand, turn-on voltage decreased as the doping concentration increased, from 5.4 to 3.9 V and from 3.9 to 3.6 V for CCDMB and PCDMB, respectively, which signifies improvement of charge injection. Overall enhancement of device performance depending on the doping concentration results from the improvement of poor hole-transporting ability of the n-type host, DPEPO, due to the shallower HOMO levels of both CCDMB and PCDMB than that of DPEPO. With the increasing doping concentration, CCDMB-based OLED exhibits a smaller CIE coordinate but PCDMB-based OLED exhibits a larger CIE coordinate (Table 4). CCDMB-doped films also showed a hypsochromic shift with the increasing doping concentration (15–35 wt%), whereas PCDMB-doped films showed a bathochromic shift with the increasing doping concentration (15–35 wt%) (Fig. S5 and Table S3). These results indicate that the CIE shift results from the molecular properties.

EQEs of the devices were measured to be 2.1% (15 wt%) and 5.5% (25 wt%) for CCDMB, and 19.8% (15 wt%) and 22.3% (25 wt%) for PCDMB, respectively (Fig. 5(c)). Devices with CCDMB dopant showed much lower efficiency than PCDMB. It is because of the low triplet harvesting ability resulting from insufficient RISC characteristic of CCDMB as discussed in transient PL diagrams in Fig. 4. However, efficient RISC in the PCDMB-based device showed high EQE of 22.3%. At the current density of  $1 \text{ mA/cm}^2$ , EL spectra showed maximum EL peaks at 440 and 500 nm, CIE of (0.16, 0.12) and (0.21, 0.45), for CCDMB and PCDMB, respectively (Fig. 5(d)).

## 4. Conclusion

We systematically discussed interrelations between the donating ability of electron donors of two emitters (CCDMB and PCDMB) and efficiencies of OLED devices. Although DFT calculations of PCDMB

showed partial overlap between the 3-substituted carbazole bridge acting as a main donor and the electron acceptor unit, the experimental  $\Delta E_{ST}$  value of PCDMB (0.13 eV) is smaller than that of CCDMB (0.21 eV). This is due to the stronger donating ability of phenoxazine than carbazole, which lowered  $S_1$  level of PCDMB and thus decreased the  $\Delta E_{ST}$ , adequate for the effective RISC. Horizontal transition dipole ratios of 76% for CCDMB and 70% for PCDMB indicate that horizontally oriented emitters become dominant. PLQYs of 25 wt% CCDMB- and PCDMB-doped DPEPO films were 63 and 65%, respectively. Transient PL decay curves of 25 wt% doped DPEPO films showed a delayed component in only PCDMB-doped film, resulting in triplet harvesting by efficient up-conversion. As a result, OLED devices fabricated with a CCDMB emitter showed deep-blue emission with CIE of (0.16, 0.12) but limited EQE<sub>max</sub> of 5.5%. PCDMB-based OLED devices showed CIE of (0.21, 0.45) and high EQE<sub>max</sub> of 22.3%.

### Declaration of competing interest

The authors declare that they have no known competing financial interests or personal relationships that could have appeared to influence the work reported in this paper.

### Acknowledgements

This work was supported by the National Research Foundation grant (No. 2021R1A2C2009088) funded by the Korea Government (MSIT).

### Appendix A. Supplementary data

Supplementary data to this article can be found online at <https://doi.org/10.1016/j.orgel.2021.106187>.

### References

- C.W. Tang, S.A. VanSlyke, Organic electroluminescent diodes, *Appl. Phys. Lett.* 51 (1987) 913–915.
- K. Mullen, U. Scherf, *Organic Light Emitting Devices: Synthesis, Properties and Applications*, Wiley-VCH, Weinheim, Germany, 2006.
- Z. Wu, N. Sun, L. Zhu, H. Sun, J. Wang, D. Yang, X. Qiao, J. Chen, S.M. Alshehri, T. Ahamad, D. Ma, Achieving extreme utilization of excitons by an efficient sandwich-type emissive layer architecture for reduced efficiency roll-off and improved operational stability in organic light-emitting diodes, *ACS Appl. Mater. Interfaces* 8 (2016) 3150–3159.
- K.S. Yook, J.Y. Lee, Organic materials for deep blue phosphorescent organic light-emitting diodes, *Adv. Mater.* 24 (2012) 3169–3190.
- H. Sasabe, J. Kido, Development of high performance OLEDs for general lighting, *J. Mater. Chem. C* 1 (2013) 1699–1707.
- M.A. Baldo, D.F. O'Brien, Y. You, A. Shoustikov, S. Sibley, M.E. Thompson, S. R. Forrest, Highly efficient phosphorescent emission from organic electroluminescent devices, *Nature* 395 (1998) 151–154.
- C. Adachi, M.A. Baldo, M.E. Thompson, S.R. Forrest, Nearly 100% internal phosphorescence efficiency in an organic light-emitting device, *J. Appl. Phys.* 90 (2001) 5048–5051.
- H.-C. Su, H.-F. Chen, F.-C. Fang, C.-C. Liu, C.-C. Wu, K.-T. Wong, Y.-H. Liu, S.-M. Peng, Solid-state white light-emitting electrochemical cells using iridium-based cationic transition metal complexes, *J. Am. Chem. Soc.* 130 (2008) 3413–3419.
- S.-C. Lo, R.E. Harding, C.P. Shipley, S.G. Stevenson, P.L. Burn, I.D.W. Samuel, High-triplet-energy dendrons: enhancing the luminescence of deep blue phosphorescent iridium(III) complexes, *J. Am. Chem. Soc.* 131 (2009) 16681–16688.
- S. Wu, M. Aonuma, Q. Zhang, S. Huang, T. Nakagawa, K. Kuwabara, C. Adachi, High-efficiency deep-blue organic light-emitting diodes based on a thermally activated delayed fluorescence emitter, *J. Mater. Chem. C* 2 (2014) 421–424.
- H. Uoyama, K. Goushi, K. Shizu, H. Nomura, C. Adachi, Highly efficient organic light-emitting diodes from delayed fluorescence, *Nature* 492 (2012) 234–238.
- H. Lim, H.J. Cheon, S.-J. Woo, S.-K. Kwon, Y.-H. Kim, J.-J. Kim, Highly efficient deep-blue OLEDs using a TADF emitter with a narrow emission spectrum and high horizontal emitting dipole ratio, *Adv. Mater.* 32 (2020), 2004083.
- T. Hatakeyama, K. Shiren, K. Nakajima, S. Nomura, S. Nakatsuka, K. Kinoshita, J. Ni, Y. Ono, T. Ikuta, Ultrapure blue thermally activated delayed fluorescence molecules: efficient HOMO-LUMO separation by the multiple resonance effect, *Adv. Mater.* 28 (28) (2016) 2777–2781.
- Y. Kondo, K. Yoshiura, S. Kitera, H. Nishi, S. Oda, H. Gotoh, Y. Sasada, M. Yanai, T. Hatakeyama, Narrowband deep-blue organic light-emitting diode featuring an organoboron-based emitter, *Nat. Photonics* 13 (2019) 678–682.
- T.-L. Wu, M.-J. Huang, C.-C. Lin, P.-Y. Huang, T.-Y. Chou, R.-W. Chen-Cheng, H.-W. Lin, R.-S. Liu, C.-H. Cheng, Diboron compound-based organic light-emitting diodes with high efficiency and reduced efficiency roll-off, *Nat. Photonics* 12 (2018) 235–240.
- Y. Liu, G. Xie, K. Wu, Z. Luo, T. Zhou, X. Zeng, J. Yu, S. Gong, C. Yang, Boosting reverse intersystem crossing by increasing donors in triarylboron/phenoxazine hybrids: TADF emitters for high-performance solution-processed OLEDs, *J. Mater. Chem. C* 4 (2016) 4402–4407.
- S. Hirata, Y. Sakai, K. Masui, H. Tanaka, S.-Y. Lee, H. Nomura, N. Nakamura, M. Yasumatsu, H. Nakanotani, Q. Zhang, K. Shizu, H. Miyazaki, C. Adachi, Highly efficient blue electroluminescence based on thermally activated delayed fluorescence, *Nat. Mater.* 14 (2015) 330–336.
- X.-D. Zhu, Q.-S. Tian, Q. Zheng, X.-C. Tao, Y. Yuan, Y.-J. Yu, Y. Li, Z.-Q. Jiang, L.-S. Liao, A sky-blue thermally activated delayed fluorescence emitter based on multimodified carbazole donor for efficient organic light-emitting diodes, *Org. Electron.* 68 (2019) 113–120.
- T.H. Kwon, S.O. Jeon, M. Numeta, H. Lee, Y.S. Chung, J.S. Kim, S.-G. Ihn, M. Sim, S. Kim, B.M. Kim, A novel design strategy for suppressing efficiency roll-off of blue thermally activated delayed fluorescence molecules through donor-acceptor interlocking by C-C bonds, *Nanomaterials* 9 (2019) 1735.
- D. Karthik, D.H. Ahn, J.H. Ryu, H. Lee, J.H. Maeng, J.Y. Lee, J.H. Kwon, Highly efficient blue thermally activated delayed fluorescence organic light emitting diodes based on tercarbazole donor and boron acceptor dyads, *J. Mater. Chem. C* 8 (2020) 2272–2279.
- F.B. Dias, S. Pollock, G. Hedley, L.-O. Pålsson, A. Monkman, I.I. Perepichka, I. F. Perepichka, M. Tavasli, M.R. Bryce, Intramolecular charge transfer assisted by conformational changes in the excited state of fluorene-dibenzothiophene-S,S-dioxide Co-oligomers, *J. Phys. Chem. B* 110 (2006) 19329–19339.
- N. Ghoneim, P. Suppan, Solvation of TICT\* states in solvent mixtures, *Pure Appl. Chem.* 65 (1993) 1739–1743.
- K. Li, Y. Liu, Y. Li, Q. Feng, H. Hou, B.Z. Tang, 2,5-bis(4-alkoxycarbonylphenyl)-1,4-diaryl-1,4-dihydropyrrolo[3,2-b]pyrrole (AAPP) AIEgens: tunable RIR and TICT characteristics and their multifunctional applications, *J. Phys. Chem. C* 116 (2012) 12187–12195.
- P. Shen, M. Li, C. Liu, W. Yang, S. Liu, C. Yang, Two sensitive fluorescent BOPIIM probes with tunable TICT character for low-level water detection in organic solvents, *J. Fluoresc.* 26 (2016) 363–369.
- R. Skaisgiris, T. Serevicius, K. Kazlauskas, Y. Geng, C. Adachi, S. Juršėnas, Origin of dual emission in  $\sigma$ -bridged donor-acceptor TADF compounds, *J. Mater. Chem. C* 7 (2019) 12601–12609.
- E. Lippert, Spektroskopische Bestimmung des Dipolmomentes aromatischer Verbindungen im ersten angeregten Singulettzustand, *Z. Elektrochem.* 61 (1957) 962–975.
- Z.R. Grabowski, K. Rotkiewicz, W. Rettig, Structural changes accompanying intramolecular electron transfer: focus on twisted intramolecular charge-transfer states and structures, *Chem. Rev.* 103 (2003) 3899–4032.
- D. Karthik, S.Y. Lee, D.H. Ahn, H. Lee, J.Y. Lee, J.H. Kwon, J.H. Park, *Org. Electron.* 74 (2019) 282–289.
- M. Wang, T. Chatterjee, C.J. Foster, T. Wu, C.-L. Yi, H. Yu, K.-T. Wong, B. Hu, Exploring mechanisms for generating spin-orbital coupling through donor-acceptor design to realize spin flipping in thermally activated delayed fluorescence, *J. Mater. Chem. C* 8 (2020) 3395–3401.
- Y. Danyliv, D. Volyniuk, O. Bezvikonnyi, I. Hladka, K. Ivaniuk, I. Helzhynskyy, P. Stakhira, A. Tomkeviciene, L. Skhirtladze, J.V. Grazulevicius, Through-space charge transfer in luminophore based on phenyl-linked carbazole- and phthalimide moieties utilized in cyan-emitting OLEDs, *Dyes Pigments* 172 (2020), 107833.
- P.L. dos Santos, M.K. Etherington, A.P. Monkman, Chemical and conformational control of the energy gaps involved in the thermally activated delayed fluorescence mechanism, *J. Mater. Chem. C* 6 (2018) 4842–4853.
- Q. Zhang, J. Li, K. Shizu, S. Huang, S. Hirata, H. Miyazaki, C. Adachi, Design of efficient thermally activated delayed fluorescence materials for pure blue organic light emitting diodes, *J. Am. Chem. Soc.* 134 (2012) 14706–14709.
- S.-Y. Kim, W.-I. Jeong, C. Mayr, Y.-S. Park, K.-H. Kim, J.-H. Lee, C.-K. Moon, W. Brutting, J.-J. Kim, Organic light-emitting diodes with 30% external quantum efficiency based on a horizontally oriented emitter, *Adv. Funct. Mater.* 23 (2013) 3896–3900.
- Y. Lee, S.-J. Woo, J.-J. Kim, J.-I. Hong, Blue thermally activated delayed fluorescence emitter using modulated triazines as electron acceptors, *Dyes Pigments* 172 (2020), 107864.